JMEPEG (2012) 21:714–720
DOI: 10.1007/s11665-012-0147-x

1059-9495/$19.00

Capillarity-Driven Infiltration of Alumina Foams with an Al-Mg Alloy: Processing, Microstructure, and Properties

R. Gil and A.R. Kennedy

(Submitted October 21, 2011; in revised form January 9, 2012)

Alumina ceramic foams have been infiltrated with an Al-10 Mg alloy, by a capillarity-driven process, to create interpenetrating composites. Infiltration maps are presented for three different foam types which depict the temperature and time required for successful infiltration. The Young's modulus of "fully" infiltrated composites containing approximately 18, 25, and 36 vol.% ceramic were measured and found to be 96, 110, and 124 GPa, respectively. Porosimetry of the foams revealed a significant fraction of closed porosity within the cell walls, the quantity of which increases with foam density, which accounts for the lower density and stiffness values that were measured, compared with those predicted by a simple model.

Keywords aluminum, interpenetrating composites, stiffness

1. Introduction

Interpenetrating composites are novel materials with potentially superior multifunctional properties compared with traditional metal matrix composites (Ref 1). It is envisaged that they could find uses as automotive pistons and connecting rods, heat sinks for electrical and electronics devices and sliding electrical contacts.

A simple route to the manufacture of these materials is the combination of the Primex™ process (Lanxide Corporation, Newark, DE, USA) for spontaneous infiltration of ceramics with an aluminum alloy and the use of open cell ceramic foams (Ref 2). Spontaneous infiltration can be achieved using an Al alloy containing Mg and a nitrogen-rich processing atmosphere. The reduction in the contact angle between the ceramic and the infiltrant, due to the high temperature, reduction of the melt surface tension by Mg, dissolution of the melt surface oxide layer and the production of more wettable solids (such as MgO, $MgAl_2O_4$, and AlN) through reactions at the metal-ceramic interface (Ref 3) all help to promote pressureless infiltration, although which factors are the most important is still under debate (Ref 4).

Although some researchers (Ref 5) claim Mg plays a key role in reducing the oxygen partial pressure to enable the alloy to infiltrate by capillary action (supported by Ref 6), others (Ref 7) dismiss that Mg helps, stating that it is not essential for infiltration. It has been said that given an absence of oxygen, the magnesium will react with nitrogen but it is not a necessary precursor reaction for infiltration. Even the role of nitrogen is underestimated (Ref 8) when it is claimed that nitridation is not needed for this infiltration process to occur. It is, however, likely that one or more of $MgAl_2O_4$, MgO, and AlN are concentrated at interfaces between alumina and the metallic phase (Ref 9-11) and that the formation of these reaction products, which are readily wetted by aluminum, could be sufficient to drive spontaneous infiltration.

Interpenetrating or co-continuous composite structures have been shown to exhibit enhanced elastic properties compared with equivalent discontinuously reinforced composites (Ref 12). Quantifying the mechanical performance of these materials and the effect of the architecture of the interpenetrating phases and different processing methods is paramount. An ability to predict the elastic modulus as a function of the volume fraction of the phases has significant merit in assisting with material selection and the design of structural components from these novel materials.

The aim of this study is to identify a processing window for the successful spontaneous infiltration of ceramic foams by an Al-Mg alloy and, for fully infiltrated preforms, to relate the Young's modulus to the ceramic foam and resulting composite structures and to a simple model developed specifically for predicting the Young's modulus of interpenetrating composites.

2. Experimental Procedure

Alumina ceramic preforms were supplied by Dytech Corporation Ltd, Derbyshire, UK, made by foaming, gelling, and sintering a slurry of ceramic powder. The fabrication process for the preforms is described elsewhere (Ref 2). The foams were supplied with nominal densities of 18, 25, and 36% of theoretical (called A18, A25, and A36, respectively) but

This article is an invited submission to JMEP selected from presentations at the Symposia "Wetting, soldering and brazing" and "Diffusion bonding and characterization" belonging to the Topic "Joining" at the European Congress and Exhibition on Advanced Materials and Processes (EUROMAT 2011), held September 12-15, 2011, in Montpellier, France, and has been expanded from the original presentation.

R. Gil, Facultad de Ingeniería, Universidad de Los Andes, Mérida, Venezuela; and **A.R. Kennedy**, Manufacturing Research Group, Faculty of Engineering, University of Nottingham, Nottingham NG7 2RD, UK. Contact e-mails: roberto_ve@yahoo.com and robertog@ula.ve.

were more accurately measured using mercury porosimetry (Autopore IV, Micromeritics, Norcross, GA, USA).

Infiltration trials were performed in a muffle furnace (Carbolite CWF 12/3 Model) in conjunction with an inconel retort. 20 mm cubes of porous alumina preforms were placed on a stainless steel mesh holder. Al-10 wt.% Mg billets, with a density of 2.530 g/cc, were cast to 18 mm diameter and sectioned to 16 mm in height and were placed on top of the preforms. As the melting point of this alloy (approx. 610 °C) is well below the infiltration temperature, a graphite tube was placed around the billet to contain it when molten. Up to six samples were loaded as part of the same run.

After loading the retort, an initial evacuation to 0.01 bar was performed using a rotary vacuum pump, followed by fast filling with nitrogen (through a chemical drier) to near-atmospheric pressure. A second purge and fill was performed before allowing nitrogen to flow through the chamber at a rate of 2 L/min. The heating cycle was set at a rate of 20 °C/min to reach the processing temperature, which was varied between 800 and 950 °C. The samples were then held at this temperature for between 30 and 120 min to allow infiltration to occur. After this, the system was allowed to cool to room temperature by switching off the furnace. The slow cooling, taking over 4 h to reach room temperature, was employed in an effort to minimize the likelihood of cracking in the sample.

The density of the infiltrated preforms was measured using a helium pycnometer (AccuPyc 1330, Micromeritics, Norcross, GA, USA). A minimum of five composite samples per ceramic content were measured. Infiltrated samples were sectioned using a diamond cutting disc, mounted in conductive bakelite resin, ground and polished for viewing in the scanning electron microscope (Jeol JSM6400, Tokyo, Japan).

The Young's modulus was measured using time-of-flight diffraction (Ref 13, 14) which is based on the relationship between the speed of sound through a particular material and its elastic constants (Ref 15). The time-of-flight of compression and shear waves travelling through the samples was visualized in a pulser receiver digitizing unit (Desktop Ultrasonic Instruments, NDT solutions, New Richmond, WI, USA), using transducers to generate the compression (TMP3 Sonatest, Milton Keynes, UK) and shear waves (V221 Olympus/Panametrics, Tokyo, Japan).

3. Results and Discussion

3.1 Preform Characterization

The secondary electron SEM images, in Fig. 1, show that the alumina foams have spherical pores linked by small windows in the cell walls (a feature of the foaming process used to manufacture these foams). It is evident from these images that as the density of the foam increases, the pore size decreases and the thickness of the cell walls increases considerably. Figure 1(d) presents a higher magnification image of the cell struts for the A36 foam, wherein it can be seen that they themselves have small pores present on the cell wall surfaces, as a result of loose packing and incomplete sintering of the sub-micron alumina powder used to make the foam.

Quantitative metallography revealed average pore sizes of roughly 140, 100, and 90 μm for the A18, A25, and A36 foams, respectively. The smallest windows between cells were roughly 10 μm, for all foams, but the size of the largest windows decreased from 70 to 30 to 20 μm as the foam density increased. The average number of windows per cell also decreased significantly as the foam density increased.

Table 1 gives the foam preform densities measured by Hg porosimetry, the bulk density determined at the lowest intrusion pressure of 2.3 kPa and the apparent or skeletal density determined at the maximum pressure of 414 MPa. The bulk densities measured by porosimetry agree closely with those measured from the dimensions and the mass of the foam preforms (0.783, 1.087, and 1.499 g/cm^3 for the A18, A25, and A36 foams, respectively). The apparent densities are significantly lower than the density for pore-free alumina, 4.05 g/cm^3 (Ref 16), indicating that the foam struts contain internal pores that are isolated from the open pore structure in the foam. The total fraction of open porosity in the preform, derived from the ratio of the bulk to apparent density, is also given in Table 1. It is clear from these data that the fraction of closed pores increases as the foam density increases, a facet of the increasing thickness of the cell struts.

Figure 2 plots the fraction infiltrated (or saturation, S) versus pressure (plotted on a logarithmic scale) for the three foams. There is a clear difference between the foam types, with higher saturation levels being achieved at lower pressures as the volume fraction of alumina in the foam decreases. These plots show the infiltration process to occur in several stages and the changing intrusion behavior with pressure can be related to the macro-, micro-, and nano-scale structures of the foam using Eq 1, Washburn's equation, where the surface tension of mercury (σ_{LV}) at 25 °C is assumed to be 0.485 N/m (Ref 17), and the contact angle for Hg on alumina to be 140°.

$$P = \frac{4\sigma_{LV}cos\theta}{d} \quad \text{(Eq 1)}$$

At low pressures, small volumes of Hg are intruded into the largest (<350 μm) surface pores. The pressure at which the slope of the curve increases corresponds to mercury being forced into pores 71, 27, and 21 μm in diameter for the A18, A25, and A36 foams, respectively. This corresponds to infiltration through the windows linking the cells, rather than the cells themselves, indicating that widespread metal flow throughout the network of interconnected pores only takes place when a pressure commensurate with that required to affect penetration through the windows between the pores is exceeded. A significant decrease in the slope of the curve, for all the three foams, occurs at a pressure of roughly 138 kPa, corresponding to a pore size of roughly 10 μm, equivalent to the pressure required to force Hg through the smallest windows. After this point, for all the foams, the saturation is weakly dependent upon pressure and it is not until pressures above roughly 5.5 MPa that the slope of the curve increases again. At this point, infiltration into the sub-micron surface pores in the cell struts occurs. The relatively large increase in volume is affected by filling larger pores contained within the struts that are accessed via these small pores. Above a pressure of roughly 10.3 MPa, for all the foams, complete filling of the open porosity occurs and the saturation reaches unity.

3.2 Characterization of the Infiltrated Preforms

The processing window was defined for all the foam preforms using multiple repeat trials under the same conditions and the results are shown in Fig. 3. Three regions were

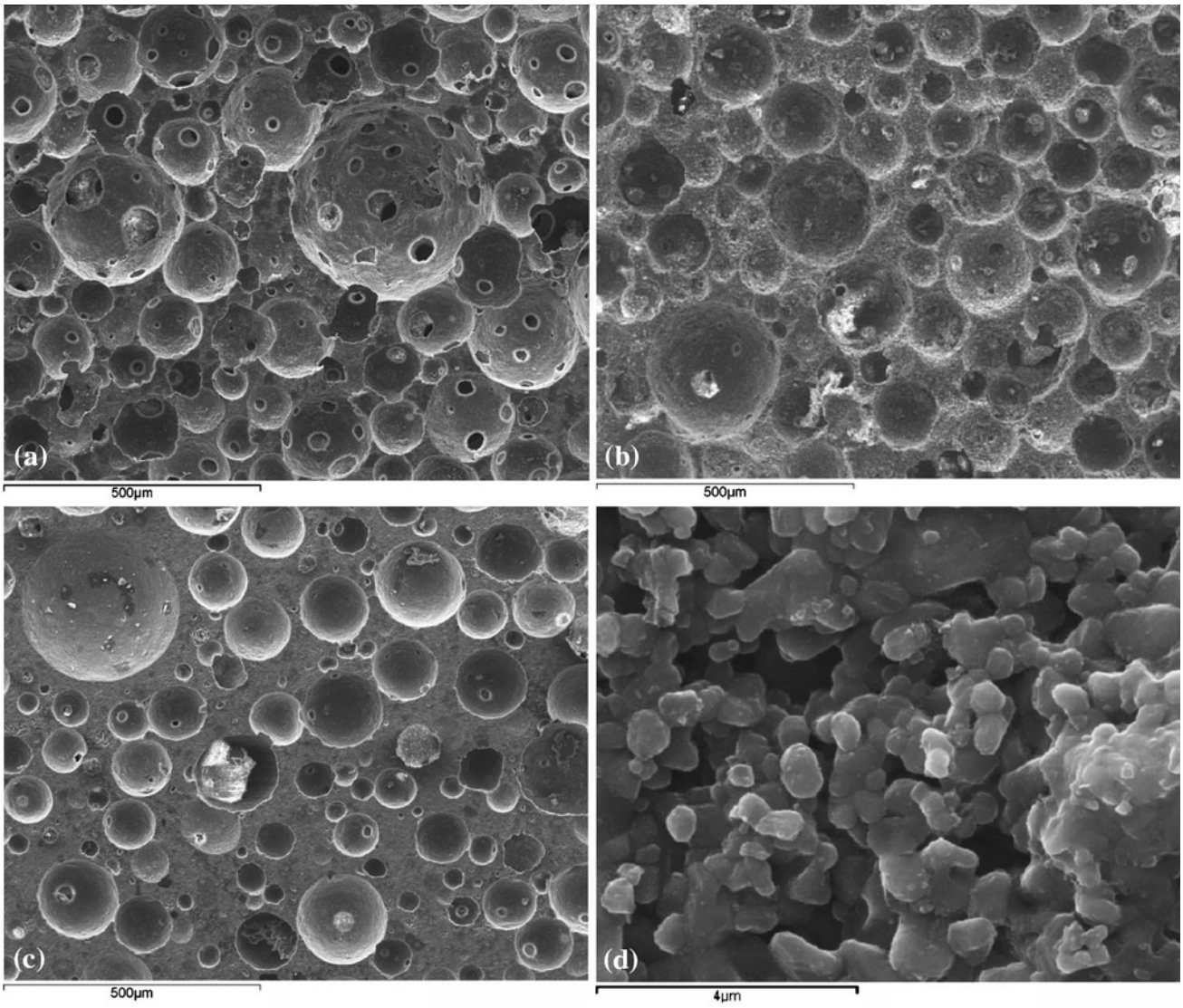

Fig. 1 SEM images of the alumina foam preforms, (a) A18, (b) A25, (c) A36, and (d) a strut in the A36 foam at higher magnification

Table 1 Densities (in g/cm^3) and fractions of porosity in the foam precursors, determined by porosimetry (the scatter is given as ±1 standard deviation)

Foam	Bulk density	Fraction of porosity	Apparent density	Open porosity	Closed porosity
A18	0.796 ± 0.001	0.803	3.755 ± 0.004	0.788	0.015
A25	1.055 ± 0.008	0.740	3.446 ± 0.009	0.694	0.046
A36	1.470 ± 0.002	0.637	3.140 ± 0.011	0.532	0.105

identified; a "no infiltration" zone where none of the trials were successful, an "infiltration" zone where all the trials were successful resulting in, what appeared to be, complete penetration of the metal into the preform, and a "transition" zone where the results were variable with some of the trials being successful and others not. As expected, infiltration is less likely to occur as the temperature is reduced, with guaranteed successful infiltration only occurring for temperatures at or above 900 °C. There is broad agreement between these observations and those for the marked decrease in surface tension, and stronger negative dependence of surface tension with increasing temperature, for molten Al in nitrogen above 830 °C. This transition is associated with reactions to form AlN above this temperature (Ref 18), supporting those studies where it is thought that the formation of AlN facilitates spontaneous infiltration (Ref 3, 9-11).

It appears that infiltration, in the case of the A25 preform, can occur quite rapidly at high temperatures (a 30 min hold was the shortest duration studied). It is possible that the lack of infiltration in some trials is due to changes of the atmosphere in the furnace chamber due to contamination or residual moisture. The dew point of the gas exiting the furnace, measured for runs without samples present since with samples in the furnace the vapors produced damaged the sensor, was seen to be very

sensitive to the cleaning and drying process for the furnace and samples as well as the process of evacuation with values in the range of +5 to −40 °C being measured.

Successful infiltration resulted in a high degree of pore filling as evidenced in the optical micrographs in Fig. 4 to 6. The arrows in these micrographs show the location of some sites of un-filled pores. The number of un-filled macro-pores observed increases as the foam density increases as the likelihood of isolation of a pore within the cell wall increases. It should be noted that all the samples were free from delamination cracking of the type observed in some similar composites (Ref 12).

Figure 7 presents a SEM image of a partially infiltrated strut in an A18 preform. Infiltration has occurred into the porous struts but the bright zones, which indicate "charging" from non-conducting regions, identify regions where metal has not penetrated the struts. Since for spontaneous infiltration small channels will be more readily filled than large ones (the opposite of when an external infiltrating pressure must be applied, such as during Hg porosimetry), it is presumed that these regions are predominant areas of closed porosity that are inaccessible to the infiltrating liquid rather than areas into which the infiltrant could not penetrate within the holding period at the infiltration temperature.

3.3 Composite Density

The densities for the "fully" infiltrated composites are given in Table 2, measured by pycnometry, and are compared with theoretically determined densities based on either filling of all the pores or filling of only the open porosity (using data from Table 1). As expected, the measured values are below those for complete filling, as the infiltrant cannot fill the closed pores in the preforms, but, unexpectedly, they are higher than those for filling of all the open porosity.

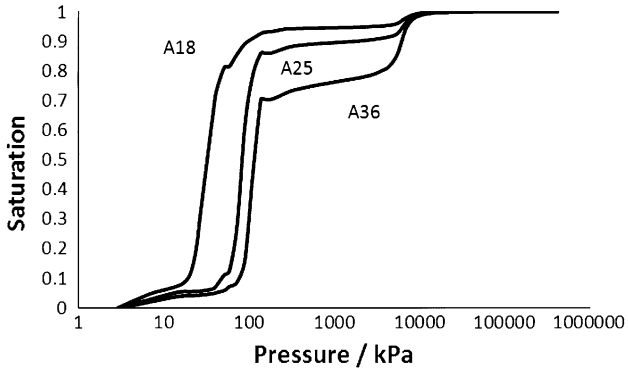

Fig. 2 Saturation versus pressure (or drainage) curves for all the foam types

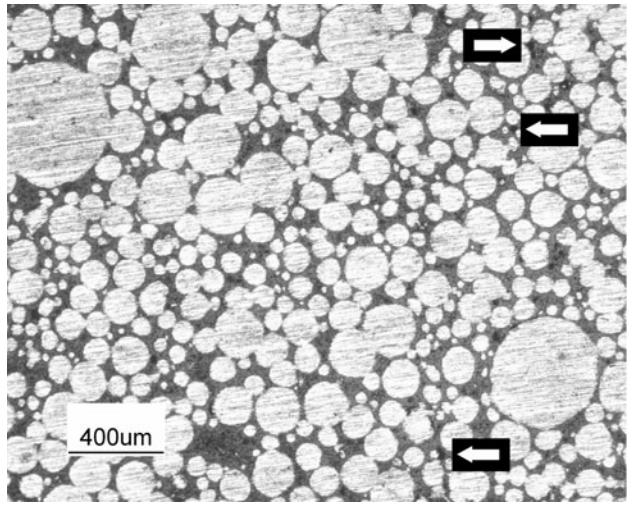

Fig. 4 Optical micrograph showing the infiltrated structure for an A18 preform. The arrows indicate un-infiltrated pores

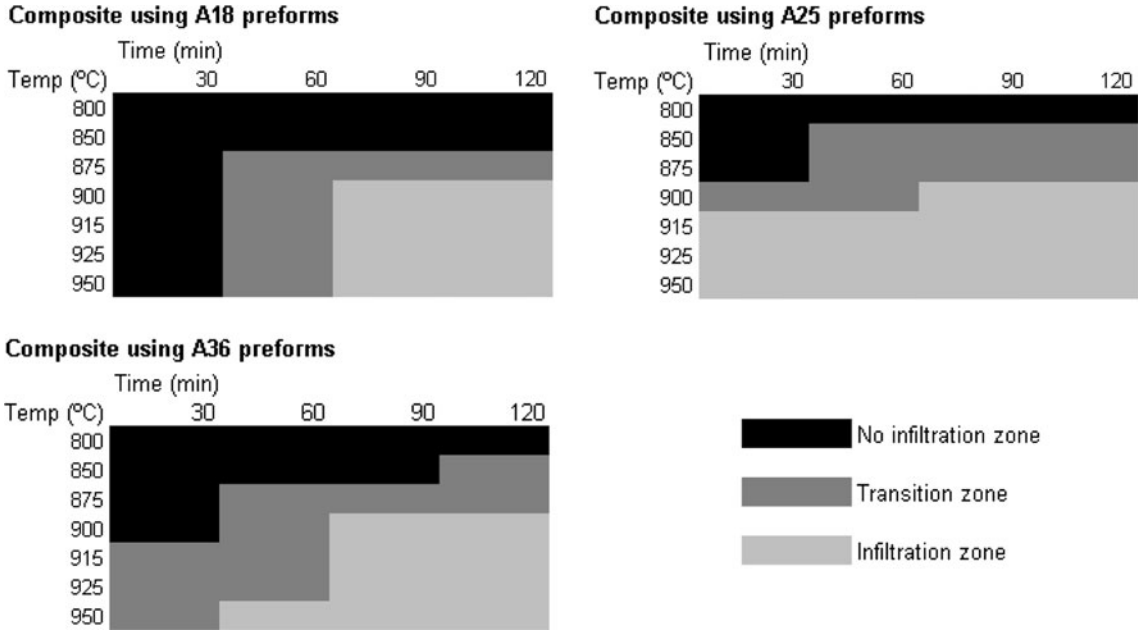

Fig. 3 Process windows for each of the ceramic foam preforms

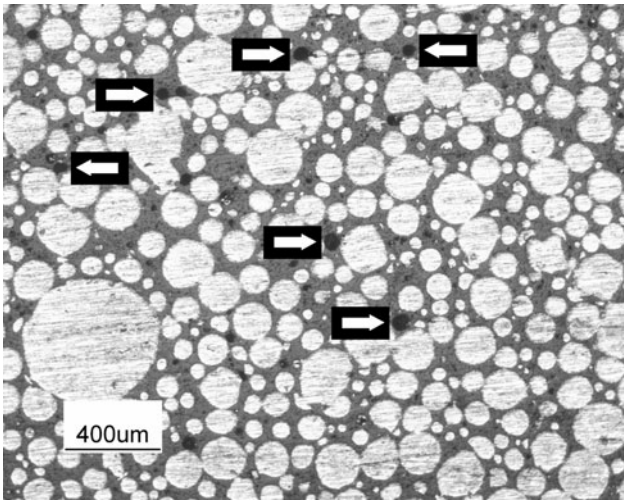

Fig. 5 Optical micrograph showing the infiltrated structure for an A25 preform. The arrows indicate un-infiltrated pores

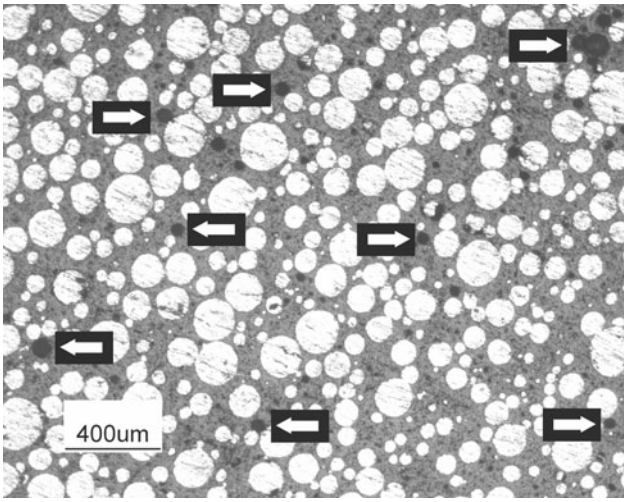

Fig. 6 Optical micrograph showing the infiltrated structure for an A36 preform. The arrows indicate un-infiltrated pores

3.4 Composite Stiffness

The Young's moduli for "fully" infiltrated A18, A25, and A36 composites were measured to be 96 ± 10, 110 ± 6, and 124 ± 6 GPa, respectively. The Young's modulus of the base Al-10 Mg alloy was measured to be 66 ± 2 GPa. These values are similar to those for equivalent interpenetrating Al-alumina composites made by squeeze casting with ceramic volume fractions between 0.17 and 0.22 (Ref 12), but are lower than those for higher volume fractions of 0.3 to 0.35 (Ref 19).

A simple model by Tuchinskii (Ref 20) was selected from the literature to compare with the experimental data. This particular model was selected as it is one of the very few models that considers a two-phase interpenetrating skeletal structure and the lower bound described by this model has been found to fit well to experimental Young's modulus data for interpenetrating composites with similar ceramic fractions to those investigated in this study (Ref 12, 19). In this model, the geometry of a cubic cell which describes the skeletal structure is related to the volume fraction of metal (f_1), and defines, in

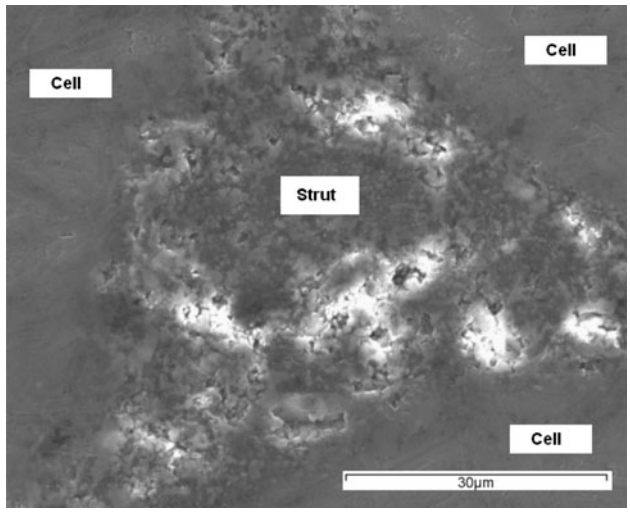

Fig. 7 SEM micrograph of a partially infiltrated strut in an A18 preform

Table 2 Experimentally measured composite densities (in g/cm^3) compared with the theoretical densities, considering either complete filling of all the pores or filling of just the open porosity

Composite	Pycnometer	Complete filling	Open pores only
A18	2.826 ± 0.032	2.828	2.790
A25	2.855 ± 0.014	2.927	2.811
A36	2.994 ± 0.043	3.082	2.816

Eq 2, a parameter t, which due to the constraints of the geometry of the model must be <1:

$$f_1 = (3 - 2t)t^2 \qquad \text{(Eq 2)}$$

The stiffness then lies between upper and lower bounds based on constraints of either isostress or isostrain. The lower bound is shown in Eq 3, where E_1 and E_2 are the Young's modulus for the metal and ceramic (skeleton), respectively. For a more complete description of this model the reader is referred to Ref 20

$$E_C^{\text{lower}} = E_2\left[(1-t)^2 + \left(\frac{E_1}{E_2}\right)t^2 + \frac{2\left(\frac{E_1}{E_2}\right)(1-t)t}{t + \left(\frac{E_1}{E_2}\right)(1-t)}\right]. \qquad \text{(Eq 3)}$$

The value selected for the Young's modulus of the ceramic, E_2, can clearly influence how well the model fits the experimental data. Although it might be assumed that the ceramic is in the form of fully dense struts, this, from porosimetry measurements, we know is not the case. An empirical model (Ref 21) has been developed which accurately predicts the stiffness of porous ceramics with structures closely resembling the porous struts in these foam preforms. It is presented in Eq 4;

$$E = E_0 \exp(-bP) \qquad \text{(Eq 4)}$$

where E_0 is the stiffness of fully dense alumina (419 GPa, Ref 21), P is the porosity of the ceramic and b was found, by experiment, to be 3.4. Figure 8 shows the relationship

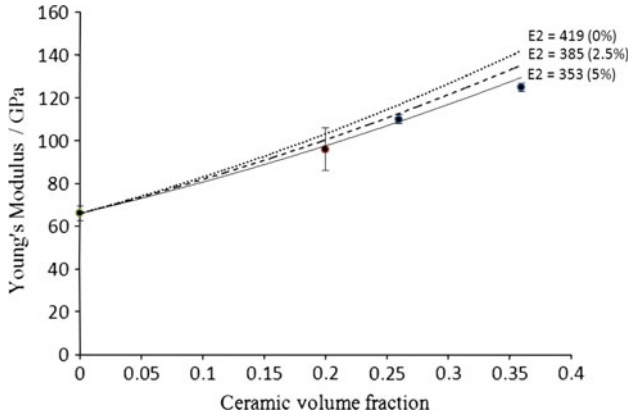

Fig. 8 Experimental Young's modulus data for interpenetrating composites as a function of ceramic content along with lower bounds predicted by the Tuchinski model (Ref 20) considering different values for the Young's modulus of the ceramic skeleton (in GPa) based on different levels of porosity therein (Ref 21)

between the experimental and the modelling data, showing predictions assuming a fully dense strut and for struts with lower Young's modulus due to different levels of porosity contained within them (marked on the plots).

The experimental data lie well below the lower bound prediction when assuming fully dense struts. This is still the case when considering struts with 2.5% porosity and a Young's modulus similar to that assumed for the skeleton structures in Ref 12, 19, 380-390 GPa (wherein these values also slightly over-predicted the Young's modulus for similar composites). A close fit, in particular at lower ceramic fractions, is observed for struts containing 5% porosity and a Young's modulus of 353 GPa.

Porosimetry has shown the ceramic foams to have complex structures and hence the resulting composites produced after infiltration consist of a metal phase which penetrates a porous ceramic skeleton containing both open porosity, most of which is infiltrated by the Al alloy and closed porosity (which of course is not). The level of porosity and fractions of open and closed porosity vary considerably with foam volume fraction. This type of structure is a deviation from the modelling assumptions which are based on 2 co-continuous phases and the deviation is expected (and observed) to be greater as the degree of porosity in the struts increases with ceramic volume fraction.

The model data can be found to fit reasonably well to the lower bound (isostrain) approach of the Tuchinskii (Ref 20) model, with judicious selection of a value for the Young's modulus of the ceramic skeleton. For rigorous modelling, this choice should be fully justified and requires calculation of the fraction of struts and determination of the strut stiffness from the volume fractions of ceramic, metal, and voids therein. As these proportions vary with the architecture of the ceramic foam, multiple calculations must be made for these unique and complex materials.

4. Conclusions

Alumina ceramic foams have been infiltrated with an Al-10 wt.% Mg alloy, by a capillarity-driven process, to create interpenetrating composites. Infiltration maps are presented for three different foam types which depict the temperature and time required for successful infiltration.

Characterization of the alumina foam preform revealed that the struts contain both the open and the closed pores and that as the density of the foam increases, so does the fraction of closed porosity. Despite the spontaneous nature of the infiltration being able to drive liquid metal into the fine pores within the struts, the high fraction of closed porosity leads to composites with lower densities than expected.

The Young's modulus of "fully" infiltrated composites was measured and found to increase with increasing ceramic fraction. Modelling, using an approach developed for interpenetrating composites, showed that good fitting to the data could only be achieved if the Young's modulus of the ceramic skeleton is decreased to compensate for the porosity contained within it.

Acknowledgments

R. Gil would like to thank the Roberto Rocca Education Program and the Universidad de Los Andes for their sponsorship. This research was supported by the Programme Alßan, the European Union Programme for High Level Scholarships for Latin America, scholarship code E07D400333VE. The authors also acknowledge the support from Dr. M. Unwin of the Ultrasonics and Digital Signal Processing Laboratory of Nottingham University.

References

1. H. Chang et al., High Strain Rate Characteristics of 3–3 Metal–Ceramic Interpenetrating Composites, *Mater. Sci. Eng. A*, 2011, **528**, p 2239–2245
2. P. Sepulveda and J.G.P. Binner, Processing of Cellular Ceramics by Foaming and In Situ Polymerisation of Organic Monomers, *J. Eur. Ceram. Soc.*, 1999, **19**(12), p 2059–2066
3. C. Garcia-Cordovilla, E. Louis, and A. Pamies, The Surface Tension of Liquid Pure Aluminium and Aluminium-Magnesium Alloy, *J. Mater. Sci.*, 1986, **21**, p 2787–2792
4. C. Garcia-Cordovilla, E. Louis, and J. Narciso, Pressure Infiltration of Packed Ceramic Particulates by Liquid Metals, *Acta Mater.*, 1999, **47**(18), p 4461–4479
5. S. Swaminathan, B.S. Rao, and V. Jayaram, The Influence of Oxygen Impurities on the Formation of AlN-Al Composites by Infiltration of Molten Al-Mg, *Mater. Sci. Eng. A*, 2002, **337**(1–2), p 134–139
6. H. Scholz and P. Greil, Nitridation Reactions of Molten Al-(Mg, Si) Alloys, *J. Mater. Sci.*, 1991, **26**, p 669–677
7. T.B. Sercombe and G.B. Schaffer, On the Role of Magnesium and Nitrogen in the Infiltration of Aluminium by Aluminium for Rapid Prototyping Applications, *Acta Mater.*, 2004, **52**(10), p 3019–3025
8. A. Zulfia, Infiltration of Al-Mg Alloy into SiC Preform in the Production of Metal Matrix Composites by Pressureless Infiltration. http://www.mrs.org/s_mrs/sec_subscribe.asp?CID=2509&DID=136455&action=detail&css=print. 17-06-10
9. C.G. Levi, G.J. Abbaschian, and R. Mehrabian, Interface Interactions During Fabrication of Aluminum Alloy-Alumina Fiber Composites, *Metall. Trans. A*, 1978, **9A**, p 697–711
10. B.S. Rao and V. Jayaram, Pressureless Infiltration of Al-Mg Based Alloys into Al_2O_3 Preforms: Mechanisms and Phenomenology, *Acta Mater.*, 2001, **49**(13), p 2373–2385
11. J. Binner, H. Chang, and R. Higginson, Processing of Ceramic–Metal Interpenetrating Composites, *J. Eur. Ceram. Soc.*, 2009, **29**, p 837–842
12. H.X. Peng, Z. Fan, and J.R.G. Evans, Bi-Continuous Metal Matrix Composites, *Mater. Sci. Eng. A*, 2001, **303**, p 37–45

13. T.K. Shen and P. Hing, Ultrasonic Through Transmission Method of Evaluating the Modulus of Elasticity of Al_2O_3-ZrO_2 Composite, *J. Mater. Sci.*, 1997, **32**, p 6633–6638
14. J.P. Charlesworth and J.A. Temple, Engineering Applications of Ultrasonic Time-of-Flight Diffraction, *Ultrasonic Inspection in Engineering Series*, M.J. Whittle, Ed., Wiley, Great Yarmouth, 1989,
15. R. Halmshaw, *Non-Destructive Testing*, 2nd ed., Edward Arnold, London, 1991, p 323
16. M. Taya and R. Arsenault, *Metal Matrix Composites: Thermomechanical Behavior*, Pergamon Press, Oxford, 1989
17. B.J. Keene, Review of Data for the Surface Tension of Pure Metals, *Int. Mater. Rev.*, 1993, **38**, p 157–192
18. R.A. Saravanan et al., Effects of Nitrogen on the Surface Tension of Pure Aluminium at High Temperatures, *Scripta Mater.*, 2001, **44**, p 965–970
19. R. Moon et al., Al-Al_2O_3 Composites with Interpenetrating Network Structures: Composite Modulus Estimation, *J. Am. Ceram. Soc.*, 2005, **88**(3), p 666–674
20. L.I. Tuchinskii, Elastic Constants of Pseudoalloys with a Skeletal Structure, *Poroshkovaya Metall.*, 1983, **247**(7), p 85–92
21. F. Ren et al., Resonant Ultrasound Spectroscopy Measurement of Young's Modulus, Shear Modulus and Poisson's Ratio as a Function of Porosity for Alumina and Hydroxyapatite, *Philos. Mag.*, 2009, **89**(14), p 1163–1182